Electronic Supplementary Material (ESI) for RSC Advances.

Ligand Functionalization of Defect-Engineered Ni-MOF-74

Jaewoong Lim,‡ Seonghwan Lee,‡ Amitosh Sharma, Junmo Seong, Seung Bin Baek* and Myoung Soo Lah*

Department of Chemistry, Ulsan National Institute of Science and Technology, Ulsan 44919, Korea

E-mail: sbbaek@unist.ac.kr; mslah@unist.ac.kr

Experimental section

General procedure

The reagents were purchased from commercial sources and used without further purification. Powder X-ray diffraction (PXRD) patterns were recorded using a Bruker D2 Phaser automated diffractometer at room temperature with a step size of 2θ = 0.02°. Solution-state ^{1}H nuclear magnetic resonance (NMR) spectra of acid digested samples in DMSO-d_6, DCl (35%), and D_2SO_4 were recorded using a Bruker 400 MHz FT-NMR spectrometer at the UNIST Central Research Facilities. The ^{1}H chemical shifts were referenced to the residual proton resonance of the DMSO-d_6 solvent in ppm. Thermogravimetric analysis (TGA) was performed using an STD Q-600 series instrument (TA Instruments Inc.) at a heating rate of 10 °C min^{-1} under an N_2 flow.

Gas adsorption measurements

Samples in amount of 20−40 mg were pretreated at 150 °C under vacuum for 24 h prior to gas adsorption measurements. N_2 adsorption/desorption isotherms were measured at 77 K using a BELSORP-Max (BEL Japan, Inc.) low-pressure adsorption measuring system employing a standard volumetric technique up to saturation pressure. The adsorption data in the pressure range of < 0.1 P/P_0 were fitted to the Brunauer–Emmett–Teller (BET) equation to determine the BET surface area using the BELMaster software (BEL Japan). CO_2 adsorption/desorption isotherms were recorded using the BELSORP-Max adsorption measuring system equipped with a temperature control unit. For all defect-engineered Ni-MOF-74 derivatives, the CO_2 adsorption isotherms were measured at 273 K up to 1 bar. For the defect-engineered derivatives selected for isosteric heat of adsorption (Q_{st}) calculations, CO_2 adsorption isotherms were recorded at 273 K, 283 K, and 293 K, respectively. All adsorption data were manipulated with BEL-Master software provided by BEL Japan Inc.

Calculation of the Isosteric heat of adsorption

Virial equation (1) was employed to calculate the isosteric heat of adsorption (Q_{st}) for CO_2 in the defect-engineered Ni-MOF-74.[S1]

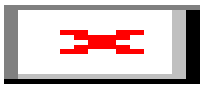

In equation (1), p is the pressure of the gas phase at equilibrium (kPa), N is the adsorbed amount per mass of adsorbent (mmol g^{-1}), T is the absolute temperature (K), a_i and b_j are virial coefficients, and m and n represent the number of coefficients required to adequately fit the isotherms. The coverage-dependent isosteric heat of adsorption Q_{st} was evaluated using equation (2).

$$Q_{st} = -R\sum_{i=0}^{m} a_i N^i \qquad (2)$$

In equation (2), R is the universal gas constant (8.314 J K^{-1} mol^{-1}). The virial coefficients were derived by fitting the experimental adsorption isotherms (ln p versus N) measured at 273 K, 283 K, and 293 K. The fitted parameter values are presented in Electronic Supplementary Information (ESI).

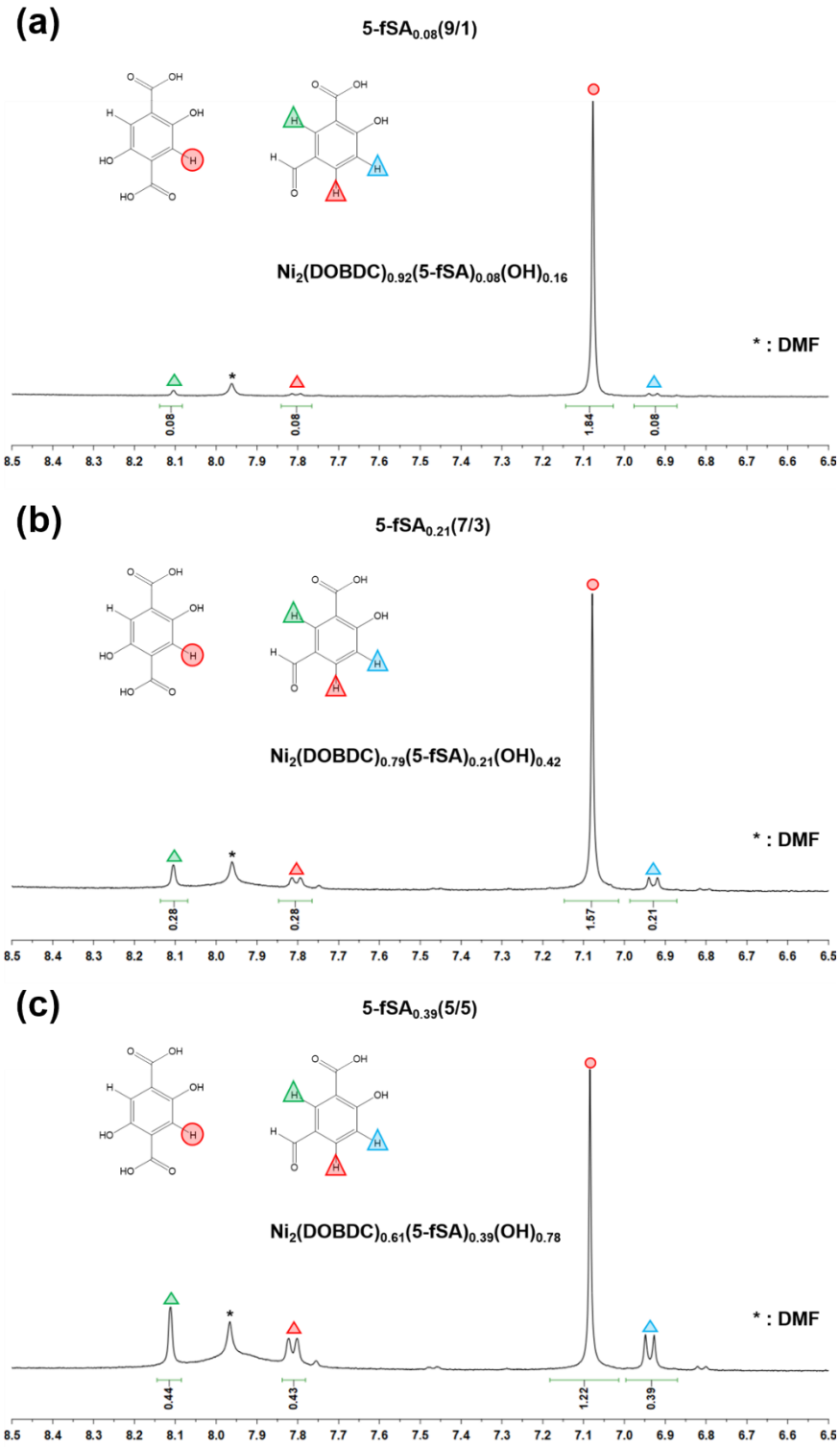

Figure S1. ^{1}H NMR spectra of acid digested **5-fSA$_x$**(a/b). (a) **5-fSA$_{0.08}$**(9/1), (b) **5-fSA$_{0.21}$**(7/3), and (c) **5-fSA$_{0.39}$**(5/5). In **5-fSA$_x$**(a/b), **x** is the estimated molar fraction of the fragmented ligand, H_2-5-fSA, in the framework from the ^{1}H NMR spectrum, and a/b is the molar ratio of H_4DOBDC and H_2-5-fSA used to prepare the defect-engineered Ni-MOF-74.

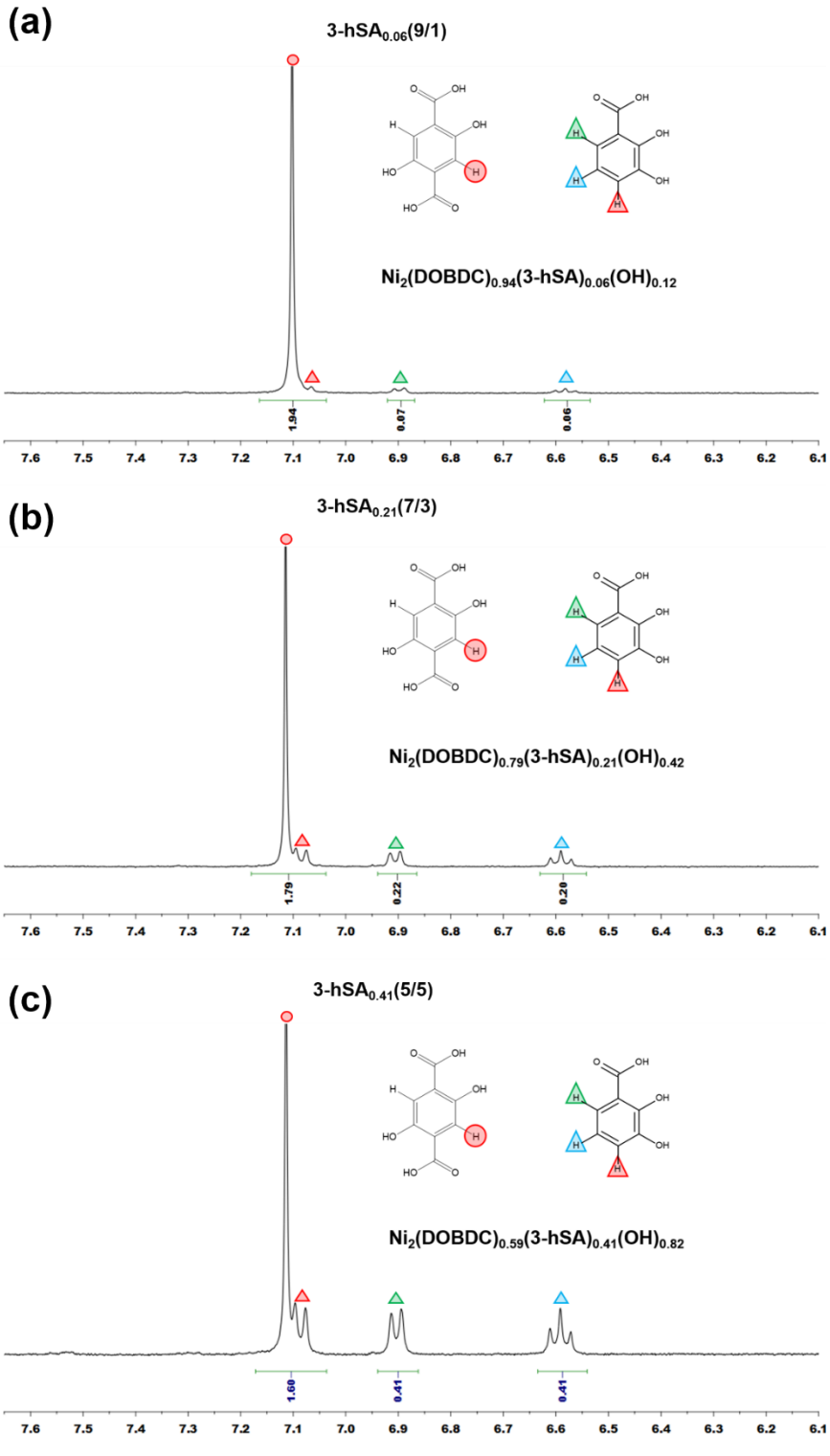

Figure S2. ^{1}H NMR spectra of acid digested **3-hSA$_x$**. (a) **3-hSA$_{0.06}$**(9/1), (b) **3-hSA$_{0.21}$**(7/3), and (c) **3-hSA$_{0.41}$**(5/5).

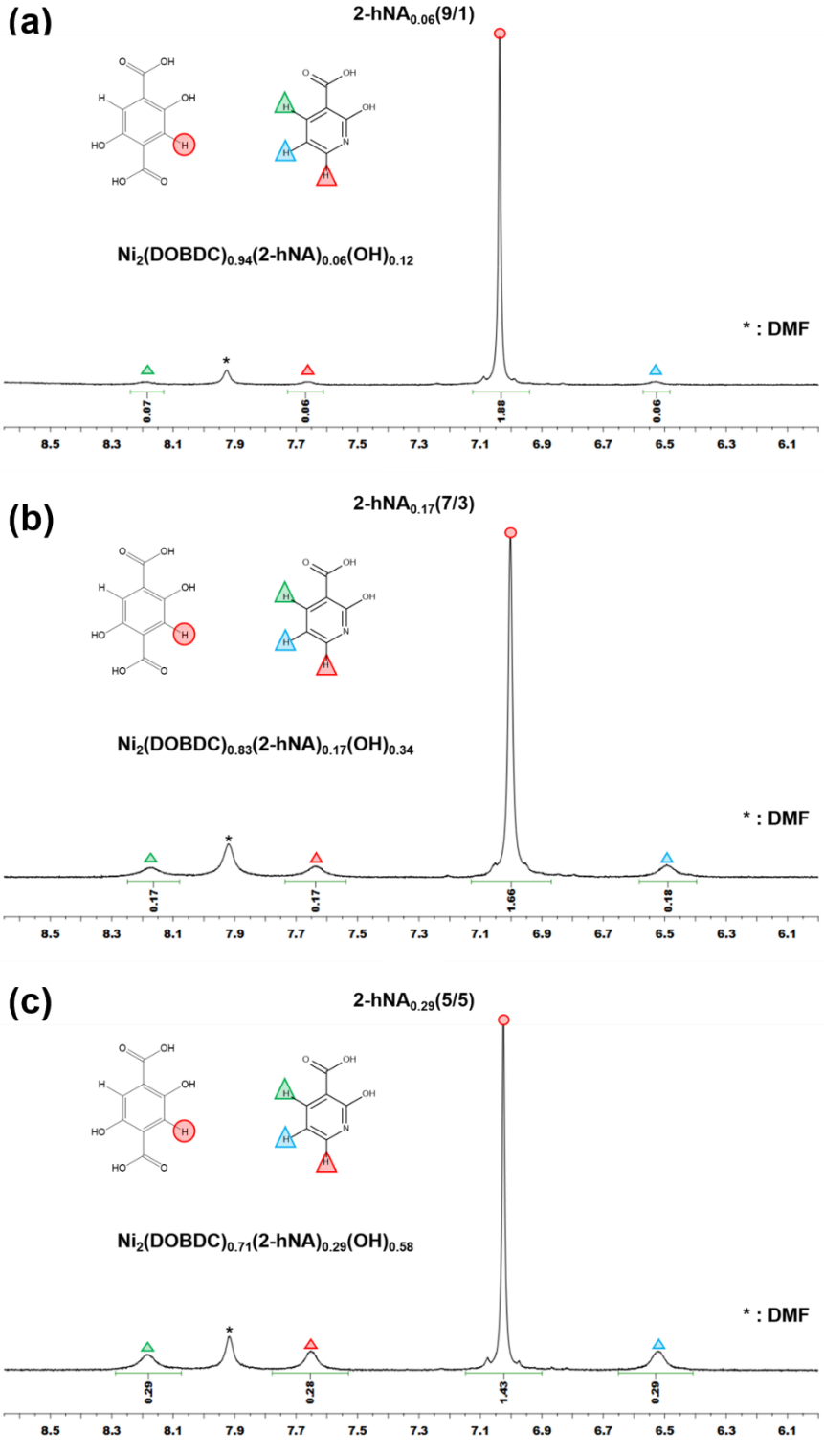

Figure S3. ^{1}H NMR spectra of acid digested **2-hNA$_x$**. (a) **2-hNA$_{0.06}$**(9/1), (b) **2-hNA$_{0.17}$**(7/3), and (c) **2-hNA$_{0.29}$**(5/5).

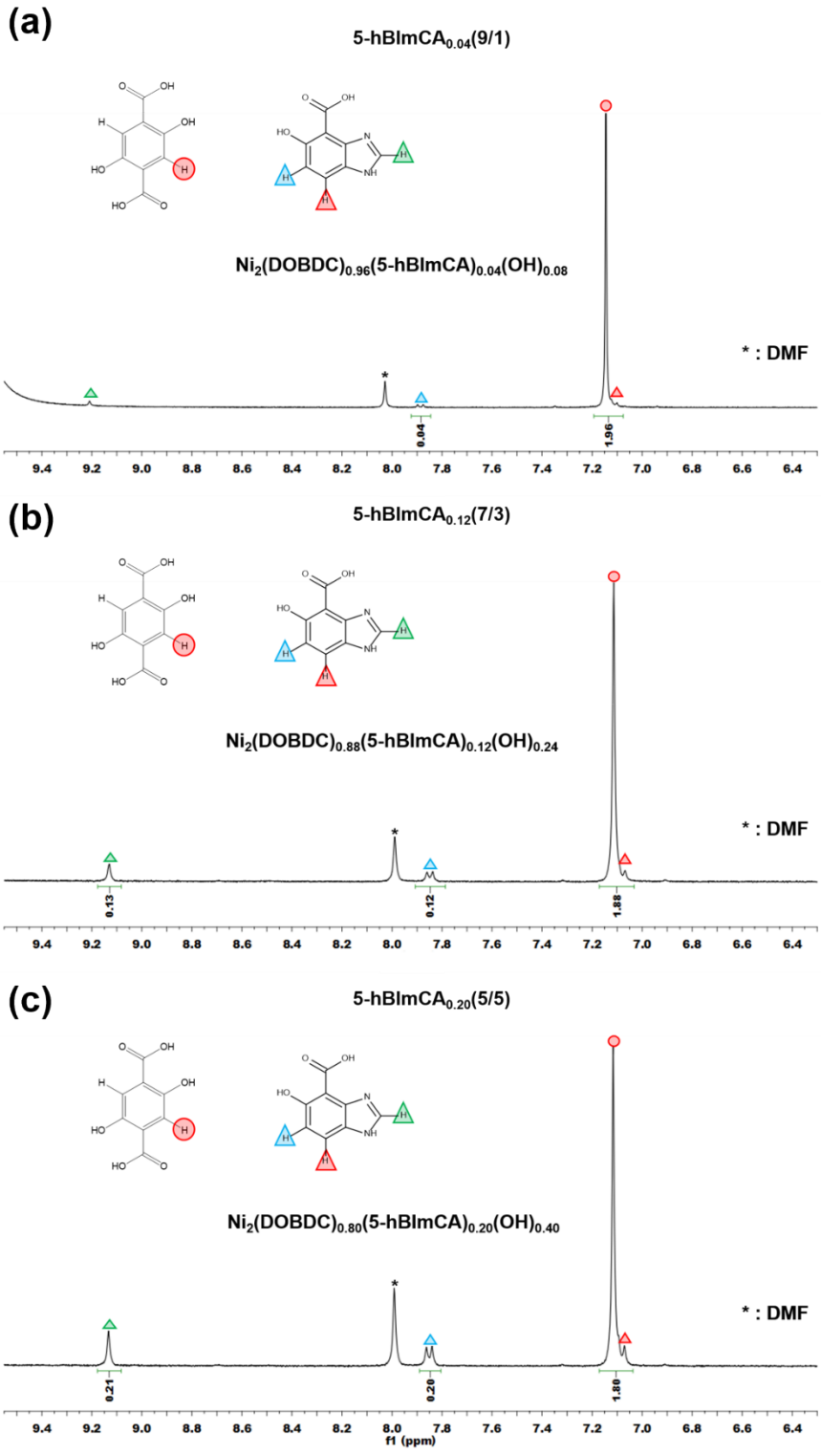

Figure S4. ^{1}H NMR spectra of acid digested **5-hBImCA$_x$**. (a) **5-hBImCA$_{0.04}$**(9/1), (b) **5-hBImCA $_{0.12}$**(7/3), and (c) **5-hBImCA$_{0.20}$**(5/5).

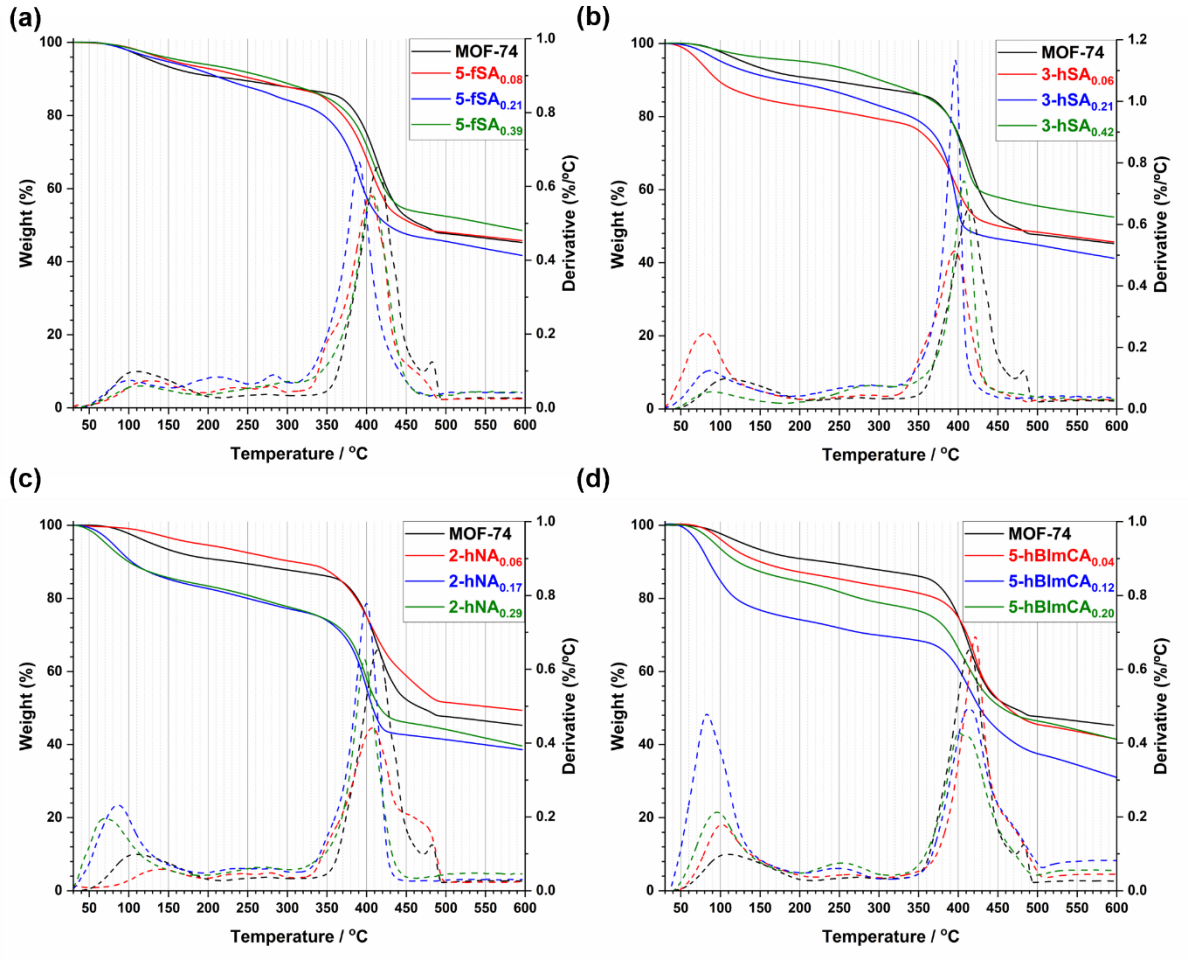

Figure S5. Thermogravimetric analysis of defect-engineered Ni-MOF-74. (a) **5-fSA$_x$**, (b) **3-hSA$_x$**, (c) **2-hNA$_x$**, and (d) **5-hBImCA$_x$**.

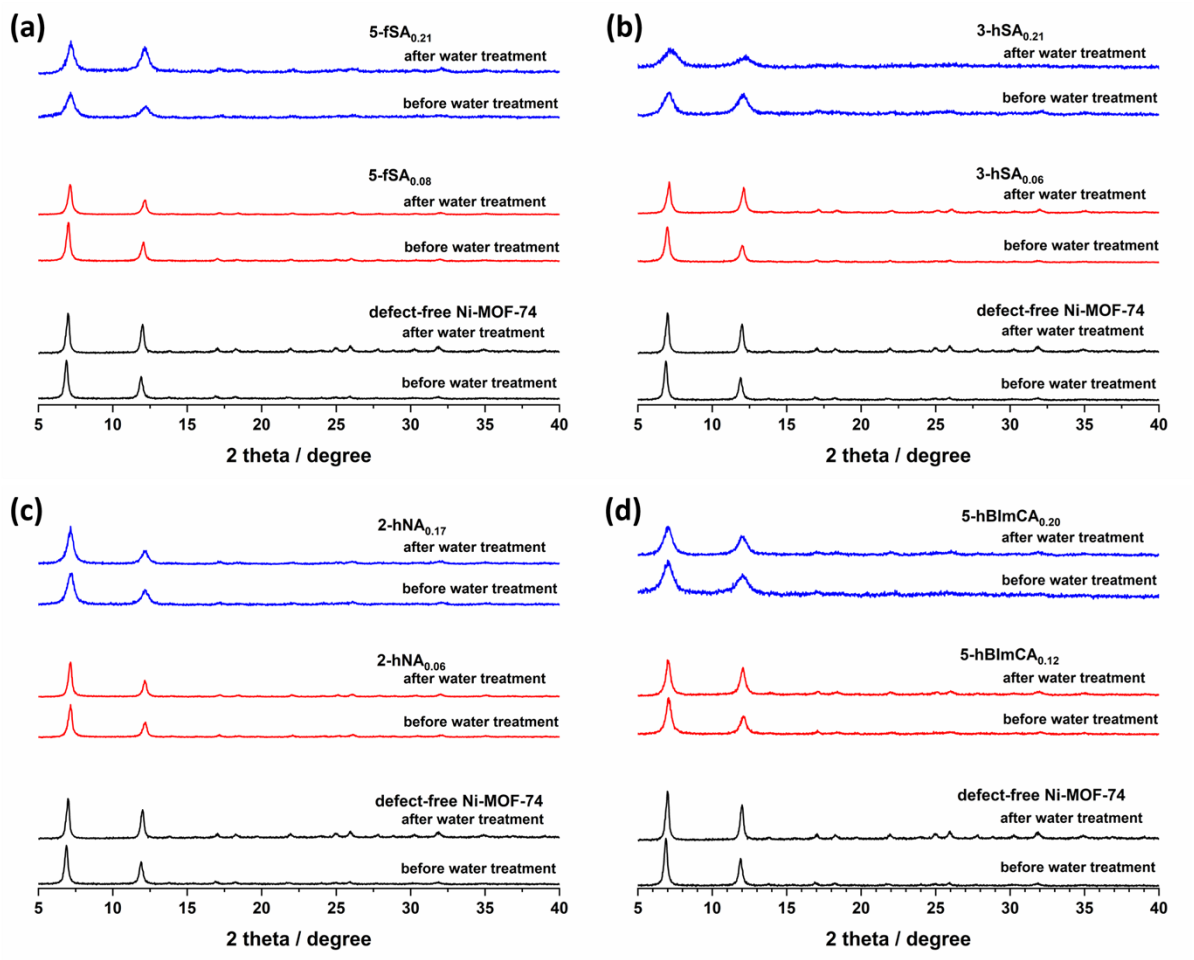

Figure S6. Comparison of PXRD patterns for defect-engineered Ni-MOF-74 before and after exposure to boilng water for 3 days. (a) **5-fSA$_x$**, (b) **3-hSA$_x$**, (c) **2-hNA$_x$**, and (d) **5-hBImCA$_x$**.

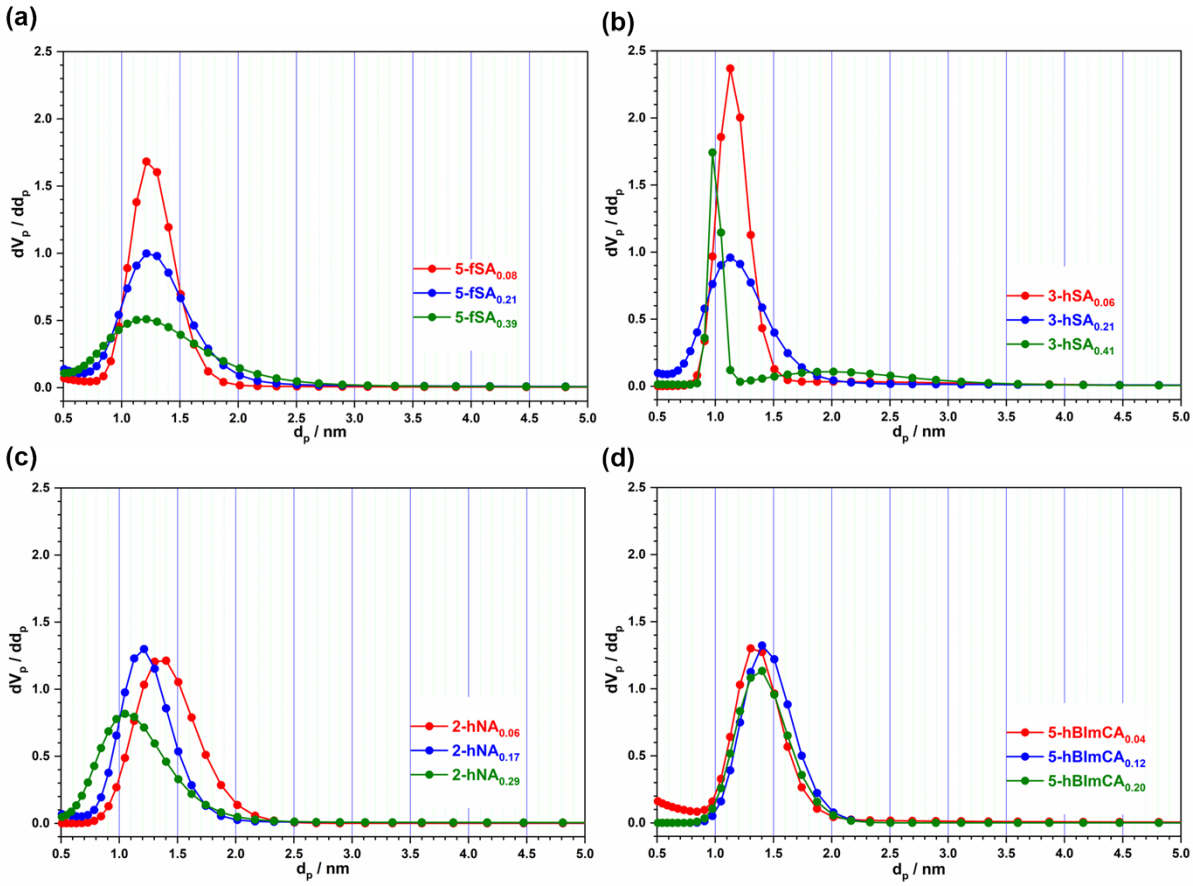

Figure S7. Nonlocal density functional theory (NLDFT) pore-size distribution of (a) **5-fSA$_x$**, (b) **3-hSA$_x$**, (c) **2-hNA$_x$**, and (d) **5-hBImCA$_x$**.

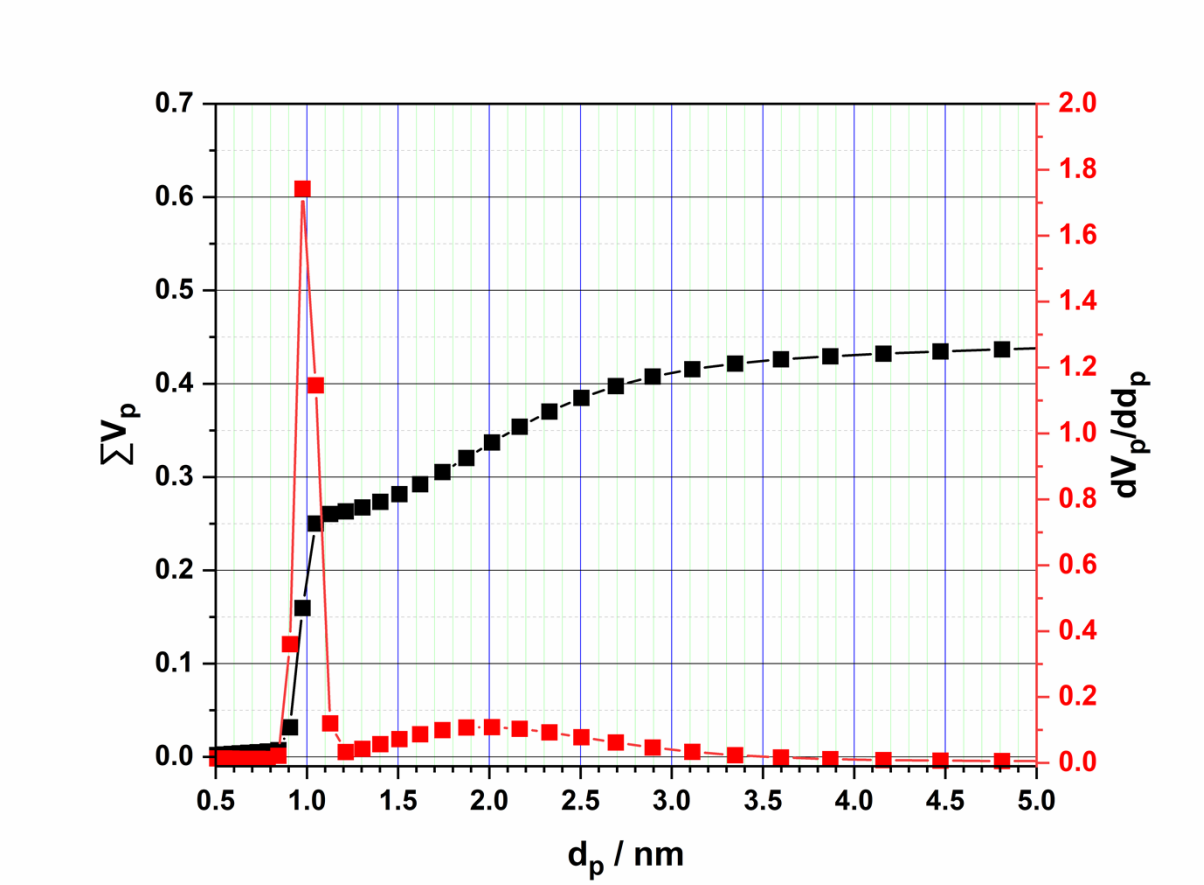

Figure S8. Nonlocal density functional theory (NLDFT) pore-size distribution and cumulative pore volume of **3-hSA$_{0.41}$**. The black line and squares represent the cumulative pore volume, and the red line and squares represent the pore-size distribution.

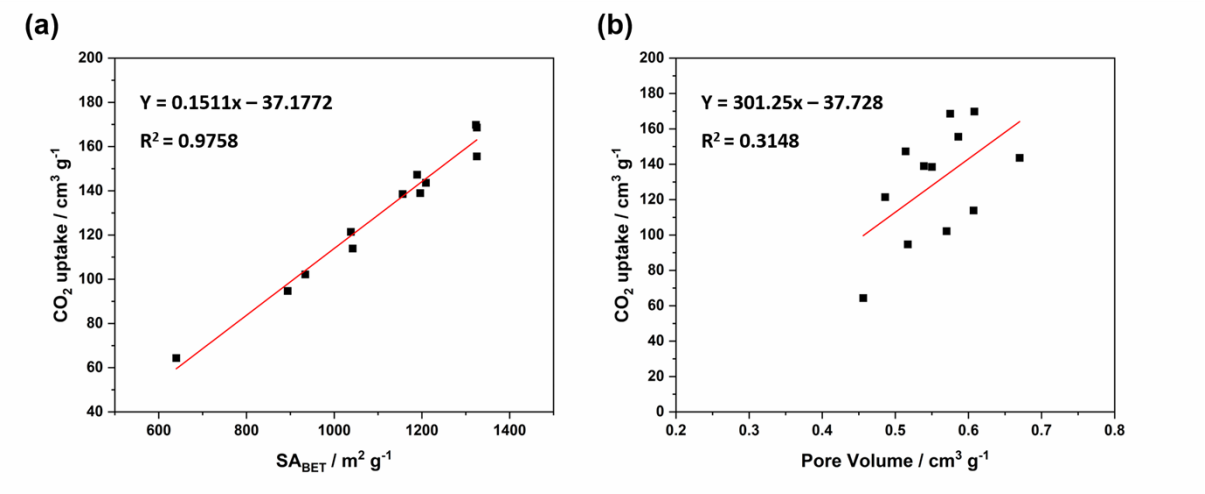

Figure S9. The overall correlation of CO_2 uptakes with (a) surface areas and (b) pore volumes of defect-engineered Ni-MOF-74 derivatives.

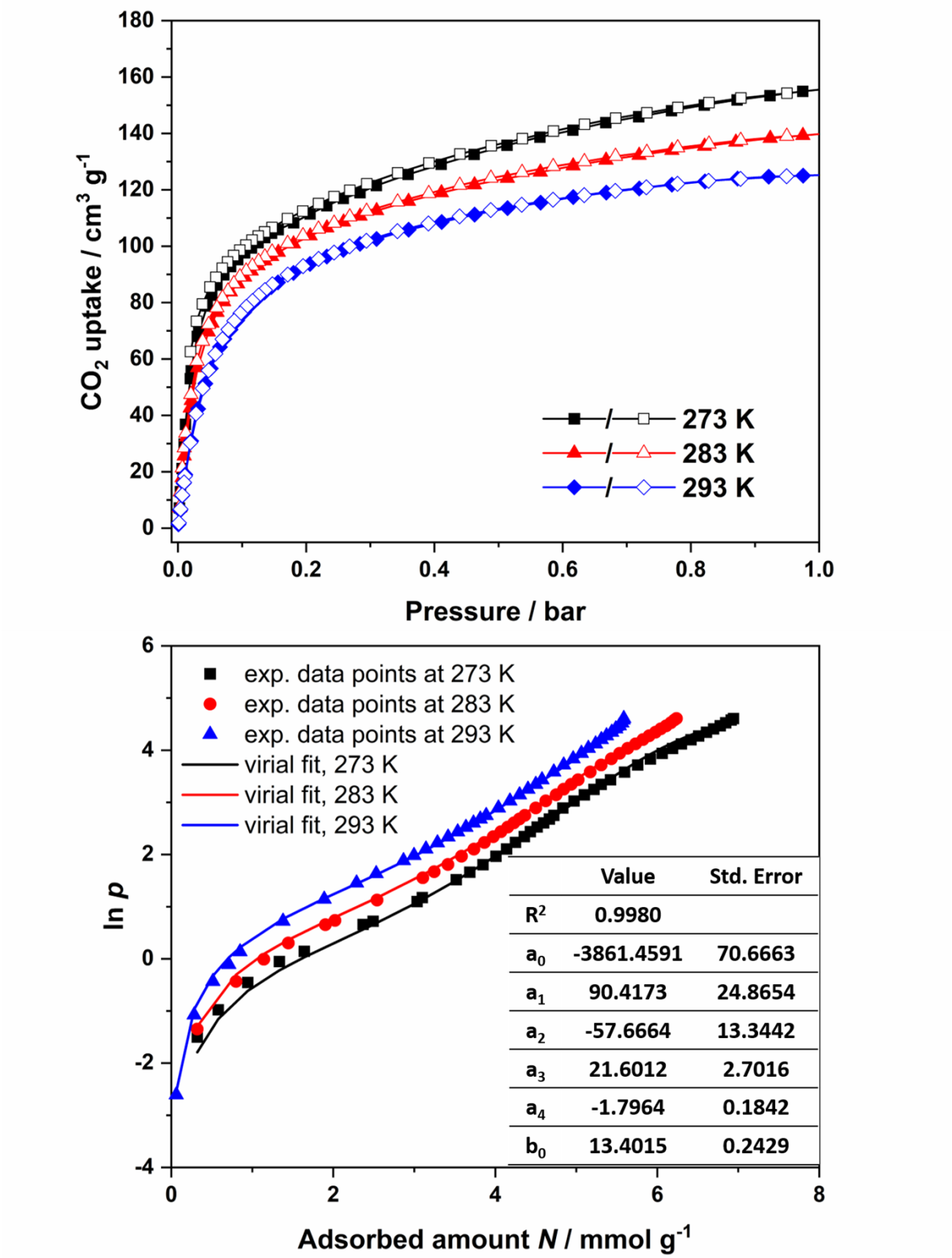

Figure S10. (a) CO_2 sorption isotherms of **5-fSA$_{0.08}$** recorded at 273 K, 283 K, and 293 K. (b) virial analysis of isotherms.

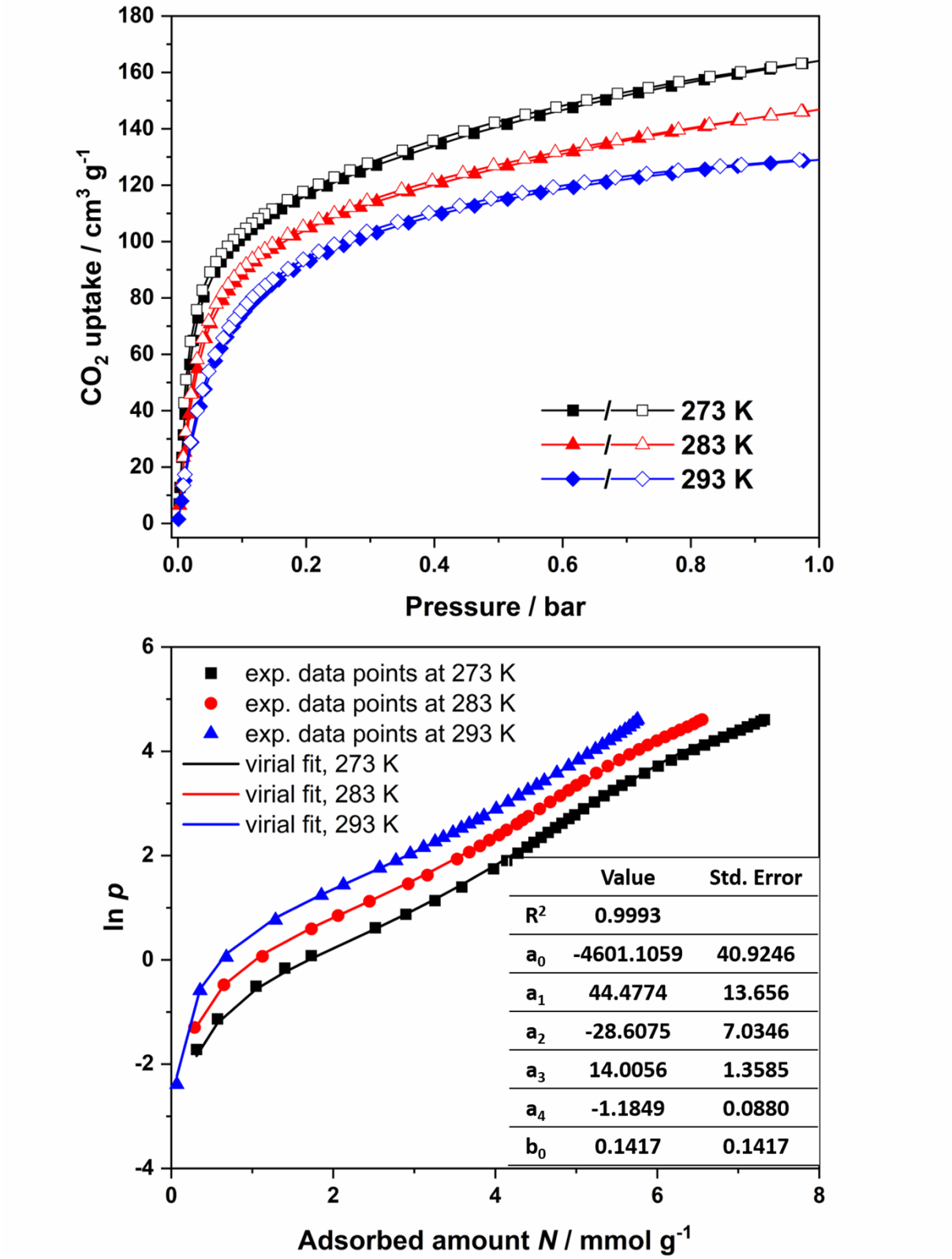

Figure S11. (a) CO_2 sorption isotherms of **5-hSA$_{0.06}$** recorded at 273 K, 283 K, and 293 K. (b) virial analysis of isotherms.

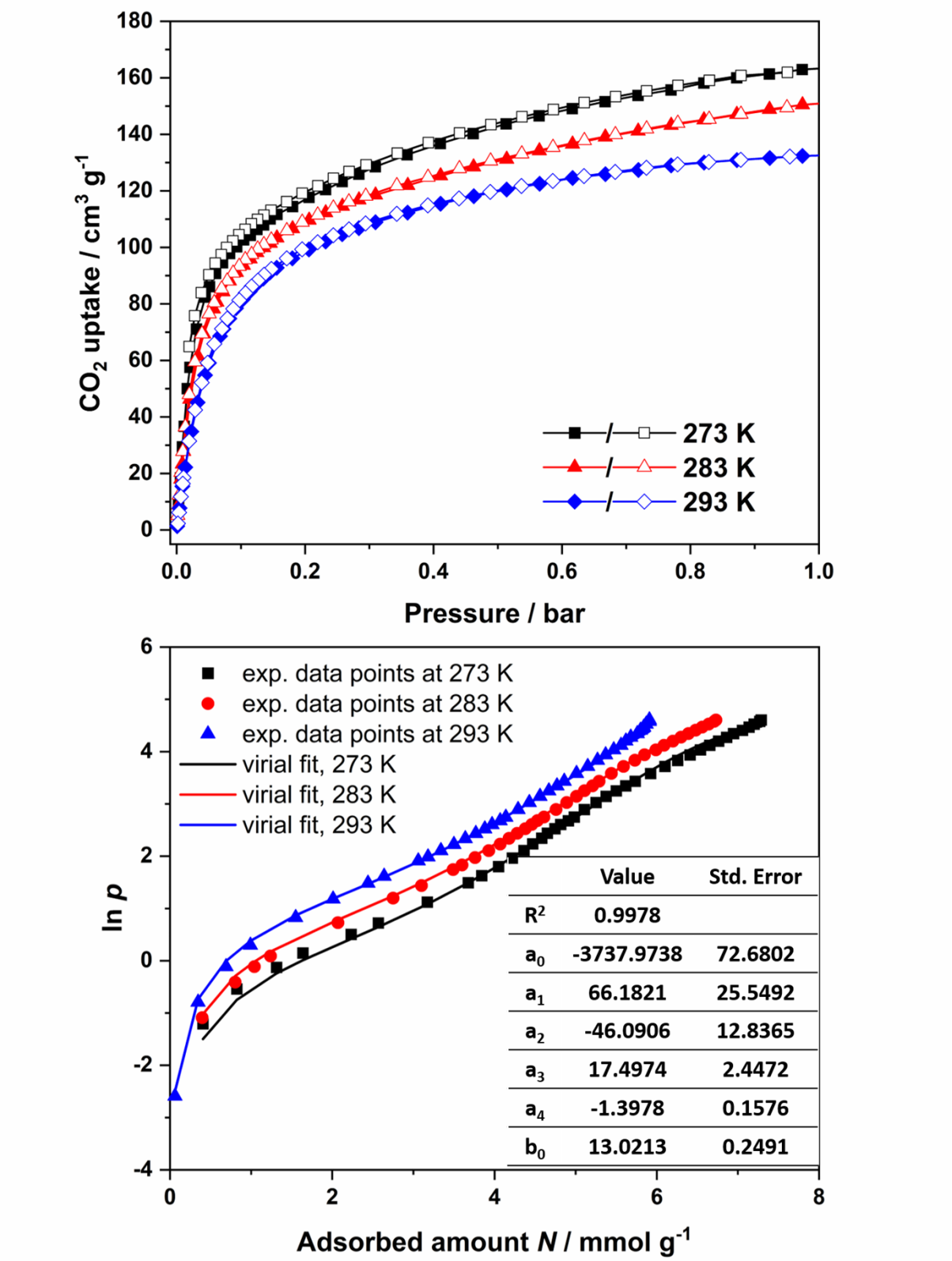

Figure S12. (a) CO_2 sorption isotherms of **2-hNA$_{0.06}$** recorded at 273 K, 283 K, and 293 K. (b) virial analysis of isotherms.

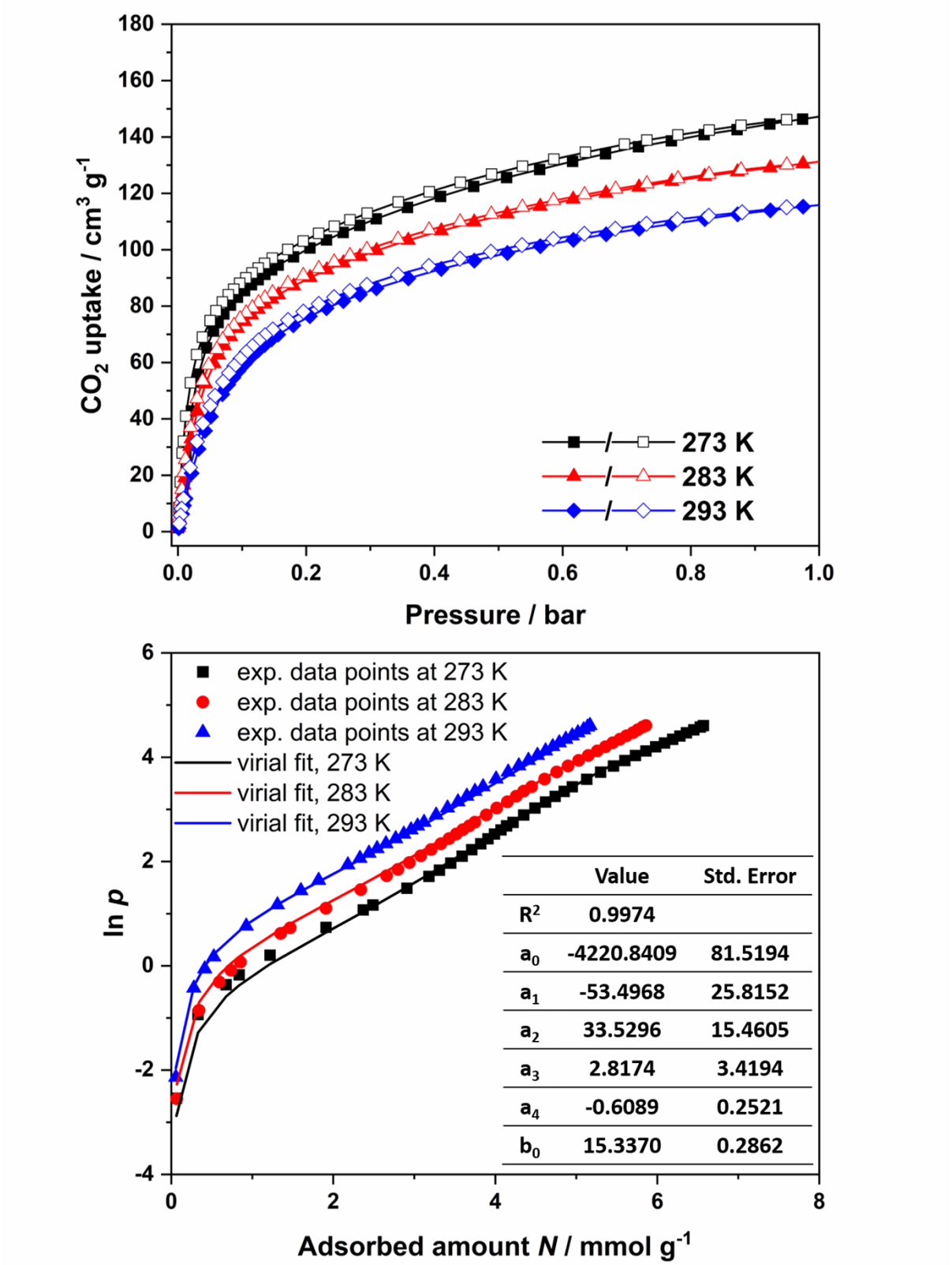

Figure S13. (a) CO_2 sorption isotherms of **5-hBImCA$_{0.12}$** recorded at 273 K, 283 K, and 293 K. (b) virial analysis of isotherms.

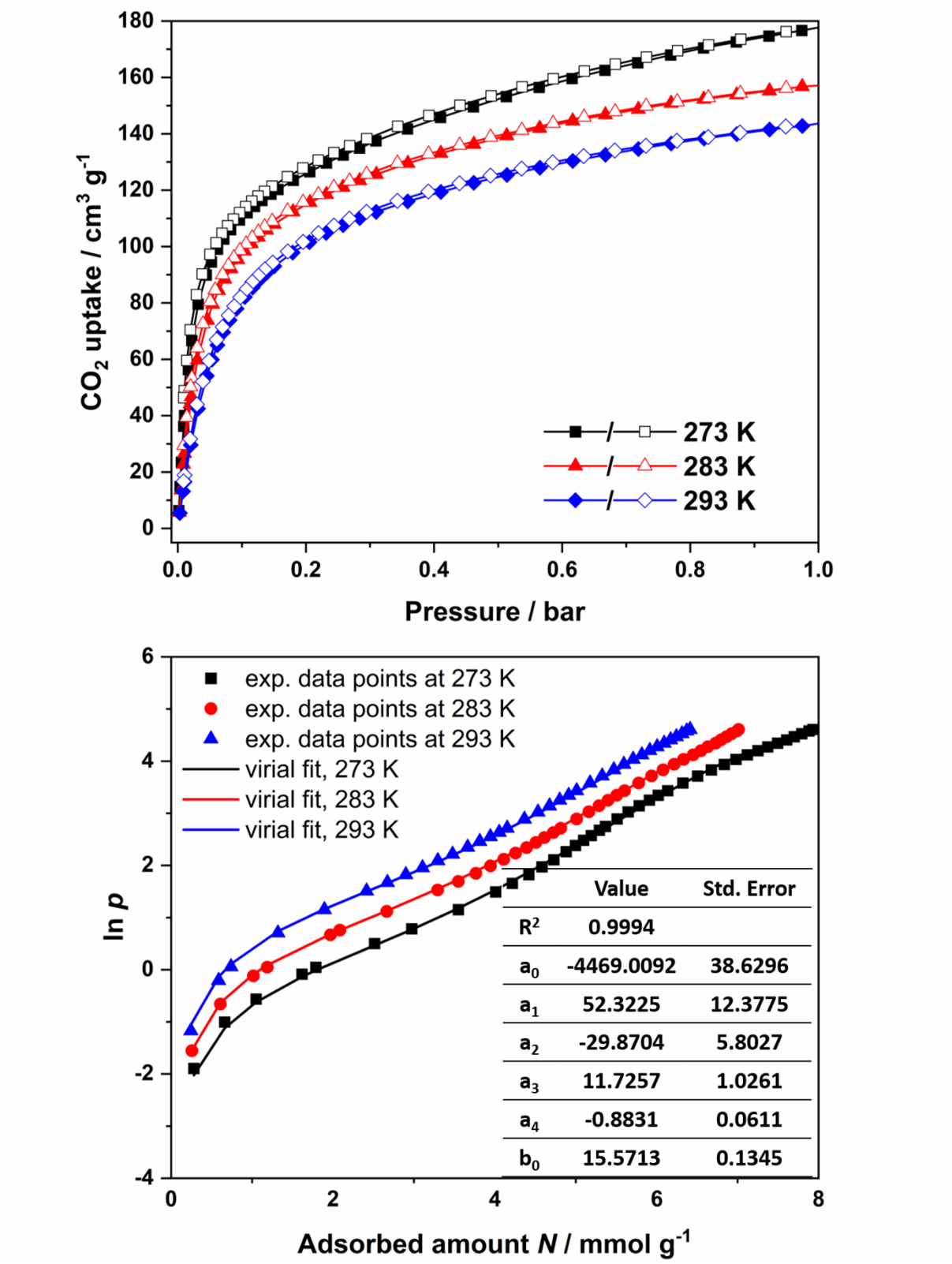

Figure S14. (a) CO_2 sorption isotherms of defect-free Ni-MOF-74 recorded at 273 K, 283 K, and 293 K. (b) virial analysis of isotherms.

Table S1. Doping ratios of fragmented ligands in the defect-engineered Ni-MOF-74.

Sample	Doping Linker	Feeding ratio/%	Doped ratio/%
5-fSA$_{0.08}$	H_2-5-fSA	10	8
5-fSA$_{0.21}$	H_2-5-fSA	30	21
5-fSA$_{0.39}$	H_2-5-fSA	50	39
3-hSA$_{0.06}$	H_2-3-hSA	10	6
3-hSA$_{0.21}$	H_2-3-hSA	30	21
3-hSA$_{0.41}$	H_2-3-hSA	50	41
2-hNA$_{0.06}$	H_2-2-hNA	10	6
2-hNA$_{0.17}$	H_2-2-hNA	30	17
2-hNA$_{0.29}$	H_2-2-hNA	50	29
5-hBImCA$_{0.04}$	H_2-5-hBImCA	10	4
5-hBImCA$_{0.12}$	H_2-5-hBImCA	30	12
5-hBImCA$_{0.20}$	H_2-5-hBImCA	50	20

Table S2. BET surface areas and pore volumes of defect-engineered Ni-MOF-74.

Sample	BET/m^2 g^{-1}	Pore volume/cm^3 g^{-1}
5-fSA$_{0.08}$	1325	0.586
5-fSA$_{0.21}$	1209	0.670
5-fSA$_{0.39}$	894	0.517
3-hSA$_{0.06}$	1323	0.608
3-hSA$_{0.21}$	1042	0.607
3-hSA$_{0.41}$	640	0.456
2-hNA$_{0.06}$	1325	0.575
2-hNA$_{0.17}$	1156	0.550
2-hNA$_{0.29}$	934	0.570
5-hBImCA$_{0.04}$	1196	0.539
5-hBImCA$_{0.12}$	1189	0.514
5-hBImCA$_{0.20}$	1038	0.486

Supplementary Reference

S1. A. Nuhnen and C. Janiak, *Dalton Trans*., 2020, **49**, 10295−10307.